Anisotropic exchange splitting of excitons affected by ΓX mixing in (In,Al)As/AlAs quantum dots: Microphotoluminescence and macrophotoluminescence measurements

J. Rautert,[1] M. V. Rakhlin,[2] K. G. Belyaev,[2] T. S. Shamirzaev,[3,4] A. K. Bakarov,[3] A. A. Toropov,[2] I. S. Mukhin,[5,6] D. R. Yakovlev,[1,2] and M. Bayer[1,2]

[1]*Experimentelle Physik 2, Technische Universität Dortmund, 44227 Dortmund, Germany*

[2]*Ioffe Institute, Russian Academy of Sciences, 194021 St. Petersburg, Russia*

[3]*Rzhanov Institute of Semiconductor Physics, Siberian Branch of the Russian Academy of Sciences, 630090 Novosibirsk, Russia*

[4]*Ural Federal University, 620002 Yekaterinburg, Russia*

[5]*St. Petersburg Academic University, Nanotechnology Research and Education Center, St. Petersburg 194021, Russia*

[6]*National Research University of Information Technologies, Mechanics and Optics (ITMO), St. Petersburg 197101, Russia*

(Received 11 October 2019; published 20 November 2019)

The anisotropic exchange splitting of the Γ exciton δ_1 is measured in (In,Al)As/AlAs quantum dots with a type-I band alignment by means of two photoluminescence techniques: The macroscopic technique exploits the competition between the anisotropic exchange interaction and the Zeeman splitting, whereas with the microscopic technique the energy splitting of the exciton fine-structure in a single quantum dot is measured directly. We find that in the spectral region of the ΓX mixing the anisotropic exchange splitting decreases strongly.

DOI: 10.1103/PhysRevB.100.205303

I. INTRODUCTION

Quantization of the motional degrees of freedom in low-dimensional semiconductor systems is interesting from the viewpoint of both basic and applied physics [1,2]. The ultimate limit of zero-dimensional carrier confinement is obtained in semiconductor quantum dots (QDs), which are attracting research attention due to their unique electronic and optical properties. A fundamental parameter of low-dimensional excitons is the fine-structure splitting that is caused by the exchange interaction, which couples the electron and hole spins [3]. In the (hypothetical) case of absence of electron-hole exchange interaction, the exciton states are fourfold degenerate in axially symmetrical QDs. A nonzero isotropic exchange interaction splits the exciton states, which are characterized by the total angular momentum projections $J_z = \pm 1, \pm 2$ on to the growth (main quantization) axis into the doubly degenerate bright and doubly degenerate dark exciton states with $J_z = \pm 1$ and $J_z = \pm 2$, respectively. Breaking of the axial symmetry in real QDs lifts the degeneracy of the bright exciton states and mixes them so that the following states emerge: $|X\rangle = \frac{1}{\sqrt{2}}(|+1\rangle + |-1\rangle)$ and $|Y\rangle = \frac{1}{i\sqrt{2}}(|+1\rangle - |-1\rangle)$ [3]. Accordingly, the anisotropic part of the electron-hole exchange interaction results also in the δ_1 splitting of the $|X\rangle$ and $|Y\rangle$ states [4]. In fact, for the majority of quantum dot systems $\delta_1 \neq 0$ [3,5,6] as size, shape, and strain anisotropies determine the fine-structure splitting.

Recently, we demonstrated the coexistence of both direct and indirect band-gap QDs with type-I band alignment in (In,Al)As/AlAs semiconductor heterostructures [7,8]. In these QDs, the Γ-valley level shifts to lower energies with increasing dot diameter more rapidly than the X-valley level due to the smaller effective mass of the Γ-valley electrons. For a particular dot diameter, the Γ- and X-electron levels cross each other leading to a change in the electron ground state. The excitons in the subensemble of direct QDs have a significant anisotropic exchange splitting δ_1, whereas the electron-hole exchange interaction is suppressed in QDs with the same shape anisotropy but an indirect band gap [9].

In this paper, we study the anisotropic exchange splitting of excitons in direct band-gap (In,Al)As/AlAs QDs with a special focus on the energy range where the Γ- and X-electron levels intersect, resulting in ΓX mixing.

II. EXPERIMENTAL DETAILS

The studied QD structure (RC1517) is a single layer of (In,Al)As QDs grown by molecular-beam epitaxy. InAs with a nominal amount of 2.7 monolayers was deposited between two 70-nm-thick AlAs barriers, leading to QD formation with type-I band alignment. Oxidation of the upper AlAs layer is prevented by a 20-nm-thick GaAs cap layer, and the light emission of the sample is enhanced by a 150-nm-thick SiO_2 antireflection coating as a cap layer. The substrate is a (001)-oriented GaAs layer, determining the growth axis z of the sample.

From the growth conditions and model calculations, we conclude that the average QD composition is given by $In_{0.64}Al_{0.36}As$ [8]. Size and density of the lens-shaped QDs were measured by transmission electron microscopy, yielding an average diameter of 16.7 nm and an amount of about 1.2×10^{10} dots per cm^2.

Two photoluminescence (PL) techniques were used to determine the anisotropic exchange splitting δ_1: (i) The macroscopic technique: Measurement of the circular polarization restoration curve of the PL line in a longitudinal magnetic

field (Faraday geometry). Here, the anisotropic exchange splitting is overcome by the Zeeman splitting, and δ_1 can be determined from the full width at half maximum (FWHM) of the polarization curve [9]. (ii) The microscopic technique: Here, the energy splitting between the linearly polarized levels is measured directly by comparing vertically and horizontally polarized PL spectra. For this purpose, a mesa structure was etched on the sample allowing spatially selective excitation of single QDs [10]. Finally, the results of both techniques are compared with each other.

For the macroscopic measurements, the sample was mounted in a liquid-helium bath cryostat with direct contact to pumped liquid helium at a temperature of $T = 1.8$ K. Magnetic fields up to 8 T were applied in Faraday geometry, parallel to the structure growth axis ($\mathbf{B} \parallel z$), using a superconducting split-coil solenoid. Nonresonant excitation above the AlAs barrier was performed using the third harmonic of a pulsed (Q-switched) Nd : YVO_4 laser with a photon energy of 3.49 eV, a repetition rate of 2 kHz, and a pulse duration of 5 ns. Selective excitation of the QDs was provided by a continuous-wave Ti:Sapphire laser tuned to an energy within the emission spectrum of the QD ensemble. In both cases, the wave vector of the exciting light was chosen to be parallel to the structure growth axis.

For time-resolved PL using nonresonant excitation in macroscopic measurements, a gated charge-coupled-device (CCD) camera synchronized with the laser was used. The time delay between the laser pulse and the start of recording t_{delay} could be varied in the range from 0 up to 500 μs. The duration of recording, i.e., the gate window t_{gate}, could be varied from 1 ns up to 500 μs in order to optimize the signal intensity and the time resolution. The best time resolution of the detection system was 1 ns.

In order to measure optical orientation, the desired circular polarizations of the exciting laser and the QD emission were selected by circular polarizers (Glan-Thompson prisms and quarter-wave plates). The PL circular polarization degree $\rho_{\mathrm{c}}^{\pm}$ following $\sigma^{\pm}$ polarized excitation is the sum of the optical orientation ρ_{oo} and the degree of circular polarization ρ_{DCP} induced by the magnetic field. It is determined through

$$\rho_{\mathrm{c}}^{\pm} = \rho_{\mathrm{oo}} + \rho_{\mathrm{DCP}} = \frac{I_{+}^{\pm} - I_{-}^{\pm}}{I_{+}^{\pm} + I_{-}^{\pm}}. \tag{1}$$

Here, $I_{\mathrm{b}}^{\mathrm{a}}$ is the intensity of the σ^{b} polarized PL emission measured after σ^{a} polarized excitation. The labels $+$ and $-$ correspond to right-hand and left-hand circular polarization, respectively.

The optical orientation is given by the difference of the circular polarization degrees measured for σ^{+} and σ^{-} polarized excitation as the effect of the magnetic field is eliminated in this way. On the other hand, the magnetic-field-induced polarization degree (DCP) is given by the average of ρ_{c}^{+} and ρ_{c}^{-},

$$\rho_{\mathrm{oo}} = \frac{\rho_{\mathrm{c}}^{+} - \rho_{\mathrm{c}}^{-}}{2}, \quad \rho_{\mathrm{DCP}} = \frac{\rho_{\mathrm{c}}^{+} + \rho_{\mathrm{c}}^{-}}{2}. \tag{2}$$

The QD photoluminescence was dispersed by a triple 1.5-m monochromator. The first and second stages of the monochromator were operated in "substractive mode" to filter the laser line out of the spectra. The PL was detected by a liquid-nitrogen-cooled CCD camera.

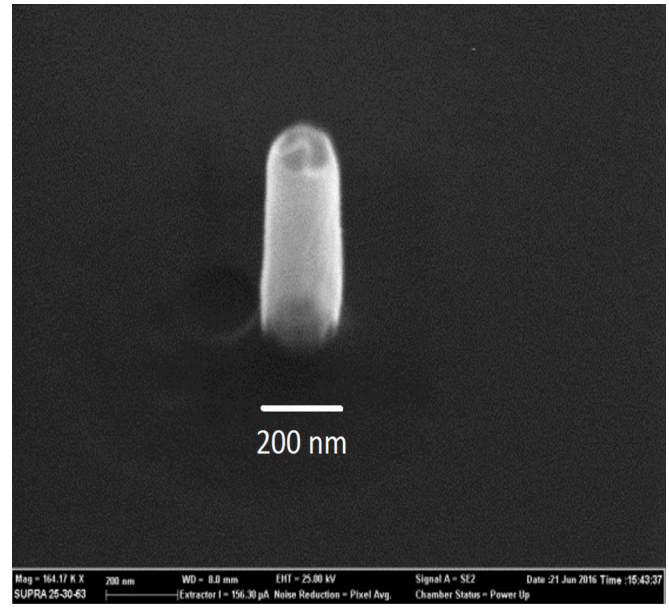

FIG. 1. Scanning electron microscope image of the mesa structure fabricated from the studied (In,Al)As/AlAs QD heterostructure.

For the microscopic measurements, the emission of a limited number of individual QDs is registered by a confocal microphotoluminescence (μPL) setup from cylindrical mesa structures of 200–500 nm in diameter, which were fabricated by electron-beam lithography and Ar^{+} ion dry etching. Scanning electron microscopy studies confirmed the formation of almost perfect cylindrical mesas with vertical sidewalls, see Fig. 1. The mesas were etched down to the buffer layer and covered with a Si_3N_4 dielectric layer to avoid the oxidation of AlAs. The average amount of QDs within a single mesa structure can be calculated with the given QD density as 4–24 dots, depending on the mesa diameter.

The sample was cooled down to 8 K in a He-flow microcryostat with an Attocube XYZ piezodriver inside, which allows us to optimize and precisely maintain the positioning of the chosen mesa with respect to the laser spot during a long time (about a few hours). The μPL and polarization measurements were performed under optical excitation by a continuous-wave laser with a photon energy of 3.07 eV. The exciting light was focused by a $\times 50$ Mitutoyo microscope objective (numerical aperture $= 0.42$) into a spot of about 10 μm in diameter. For the presented data, the power density on the sample surface can be estimated as 4 W cm^{-2}. For linear polarization measurements, we used a Glan-Taylor prism and an achromatic half-wave plate.

Time-resolved measurements on the mesa structures were performed with a pulsed semiconductor laser (photon energy: 3.07 eV, pulse duration: 20–30 ps, repetition rate: 30–50 MHz). The exciton recombination dynamics was detected with a Si single-photon avalanche diode (Micro Photon Devices) with the full width at half maximum timing resolution in the time-correlated single-photon counting mode of about 40 ps. Emission lines from individual QDs were selected by a tunable bandpass filter.

III. EXPERIMENTAL RESULTS

Recently, we demonstrated that the coexistence of (In,Al)As/AlAs QDs with direct and indirect band gaps [see Fig. 2(a)] within the ensemble is evidenced by the spectral dependence of the exciton recombination times. The indirect QDs are characterized by long decay times due to their small exciton oscillator strength. On the contrary, in direct QDs, the excitons recombine within a few nanoseconds [9,11,12]. Here, we use time-resolved photoluminescence to select direct band-gap QDs.

Photoluminescence spectra of the (In,Al)As/AlAs QD ensemble measured under nonresonant excitation are shown in Fig. 2(b). The time-integrated spectrum (black line) has a maximum at 1.67 eV and extends from 1.52 to 1.82 eV, having a FWHM of 140 meV. The large width of this emission band is due to the dispersion of the QD parameters since the exciton energy depends on QD size, shape, and composition [8].

For the spectrum measured immediately after the laser pulse ($t_{\text{delay}} = 0$ and $t_{\text{gate}} = 10$ ns), the PL band has a maximum at 1.6 eV and a FWHM of 90 meV only (red line). For longer delays ($t_{\text{delay}} = 500$ ns and $t_{\text{gate}} = 450$ μs), the emission maximum shifts to 1.68 eV, and the line broadens to 130 meV (blue line) so that it becomes rather similar to the time-integrated PL spectrum. We demonstrated recently that after the photoexcitation in the AlAs barriers, electrons and holes are captured in the QDs within several picoseconds, and the capture probability does not depend on the QD size and composition [13]. Therefore, we suggest that all QDs in the ensemble (direct and indirect) become equally populated shortly after the excitation pulse. Thus, the exciton recombination dynamics is fast for direct QDs emitting mainly in the spectral range of 1.50–1.75 eV and slow for the indirect QDs emitting in the 1.55–1.82-eV range. The emission of the direct and indirect QDs overlaps in the range of 1.55–1.75 eV.

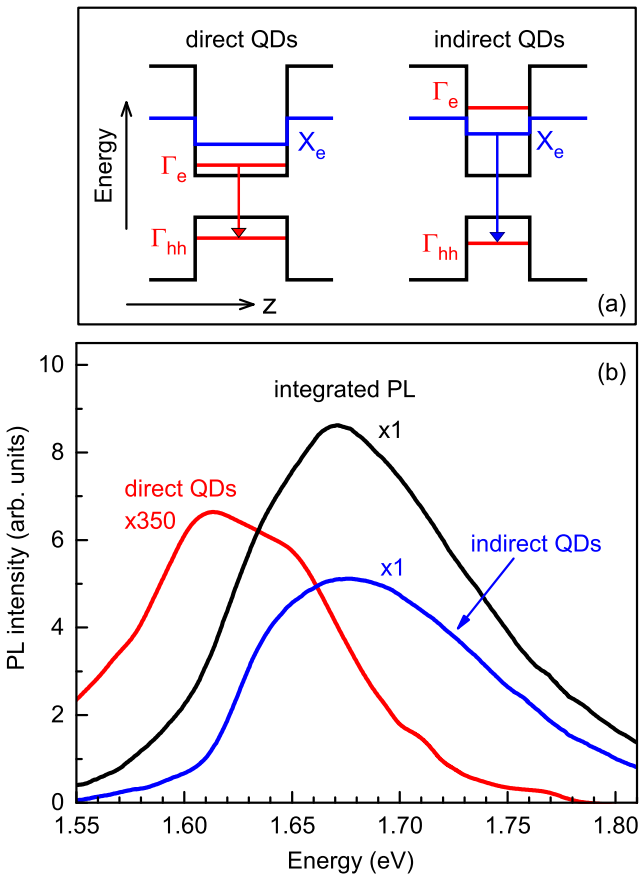

FIG. 2. (a) Band diagrams of (In,Al)As/AlAs QDs with different sizes. Γ- and X-valley energies for electron (e) and heavy hole (hh) are shown. The emission is indicated by arrows. (b) Photoluminescence spectra of (In,Al)As/AlAs QDs measured under nonresonant excitation: Time-integrated (black line) as well as time-resolved for $t_{\text{delay}} = 0$ and $t_{\text{gate}} = 10$ ns (red) and for $t_{\text{delay}} = 500$ ns and $t_{\text{gate}} = 450$ μs (blue). $T = 1.8$ K.

To distinguish between direct and indirect QDs in this spectral range, we used selective excitation within the PL emission band [9,14]. In this case, the broad emission spectrum detected under nonresonant excitation is transformed into a spectrum with narrow lines as shown in Fig. 3(a). Tuning the laser energy E_{exc} across the spectral range of the QD emission, we measured the dependencies of the peak energies of the emission from the QDs with both direct and indirect band gaps as functions of E_{exc}, which are presented in Fig. 3(b). Below $E_{\Gamma X}^{\text{low}} = 1.611$ eV, the PL spectrum consists of the direct QDs emission D (orange squares) and several phonon replicas (black symbols). The involved phonons can be identified as the longitudinal optical phonons of InAs LO_{InAs} (30 meV) and of AlAs LO_{AlAs} (50 meV) [15]. In Fig. 4(a), the spectra are presented in detail, measured in a magnetic field of 1 T. Note that the magnetic field does not affect the fundamental shape of the spectra [9]. For high excitation energies $E_{\text{exc}} > E_{\Gamma X}^{\text{low}}$, the X valley of the conduction band is below the Γ valley, and the indirect QD emission ID_{low} [cyan triangles in Fig. 3(b)] dominates the PL spectrum as shown in Fig. 4(b). Another ΓX transition occurs at $E_{\Gamma X}^{\text{high}} = 1.657$ eV. The PL peak energies of this second indirect transition ID_{high} are shown with green triangles in Fig. 3(b). The energies of ID_{low} and ID_{high} can be interpolated by the following linear functions:

$$E_{\text{det}}^{\text{low}}\,(\text{eV}) = 0.450 \times E_{\text{exc}} + 0.886, \tag{3}$$

$$E_{\text{det}}^{\text{high}}(\text{eV}) = 0.464 \times E_{\text{exc}} + 0.888. \tag{4}$$

The reason for the existence of two indirect transitions in the studied sample is not fully understood yet. Finally, there is a PL line NR_{low} at $E \approx E_{\Gamma X}^{\text{low}}$ that does not shift with the laser energy. Thus, one can see that there are two subensembles of QDs with an intersection of the Γ and X electronic levels (shown by the vertical arrows).

A. Measurements on ensemble of QDs

In order to evaluate the anisotropic exchange splitting of excitons in direct QDs with a specific size/excitation energy by the macroscopic technique, the recovery curve of the optical orientation in a longitudinal magnetic field is measured. Here, the Zeeman splitting between the $|-1\rangle$ and $|+1\rangle$ exciton states exceeds the energy of the anisotropic exchange interaction δ_1, which mixes these states. The mixing of the

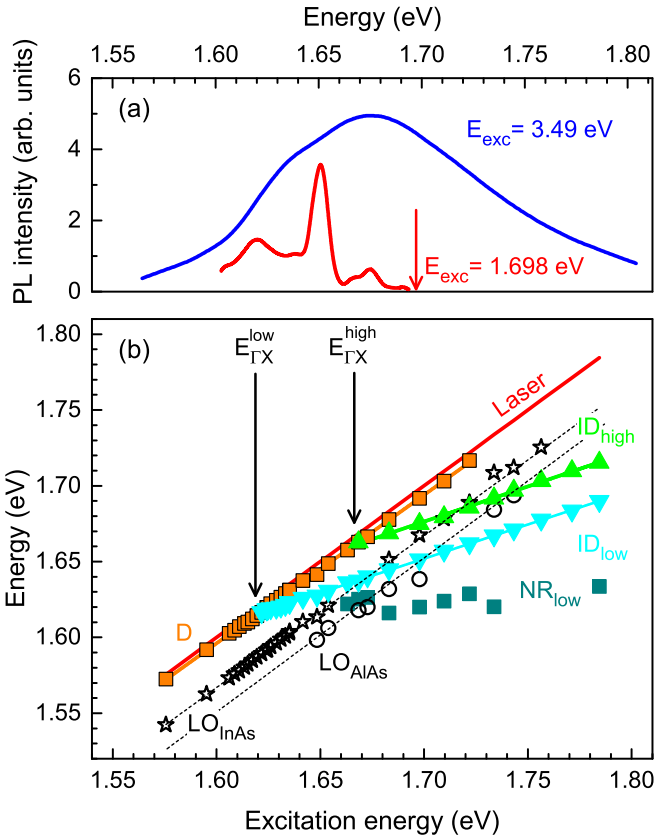

FIG. 3. (a) Time-integrated PL spectrum of (In,Al)As/AlAs QDs measured for nonresonant excitation (blue line) and PL spectrum of QDs measured for selective excitation (red line). (b) Energy positions of the PL lines plotted as functions of the selective excitation energy. Symbols give the energies of the PL lines: Excitons in direct QDs (D line, orange squares), longitudinal optical- (LO-) phonon-assisted emission from direct QDs: LO_{AlAs} (open circles) and LO_{InAs} (open stars). Excitons in indirect QDs: Low-energy line (ID_{low} line, cyan triangles) and high energy line (ID_{high} line, green triangles), nonresonant PL line (NR_{low}, dark cyan squares) which does not move with varying laser energy. Dashed lines are guides for the eye. Solid lines: Red one is laser energy, cyan and green are fits using Eqs. (3) and (4), respectively. Vertical arrows $E_{\Gamma X}^{low}$ and $E_{\Gamma X}^{high}$ mark the ΓX-crossing energies. $B = 0$ T and $T = 1.8$ K.

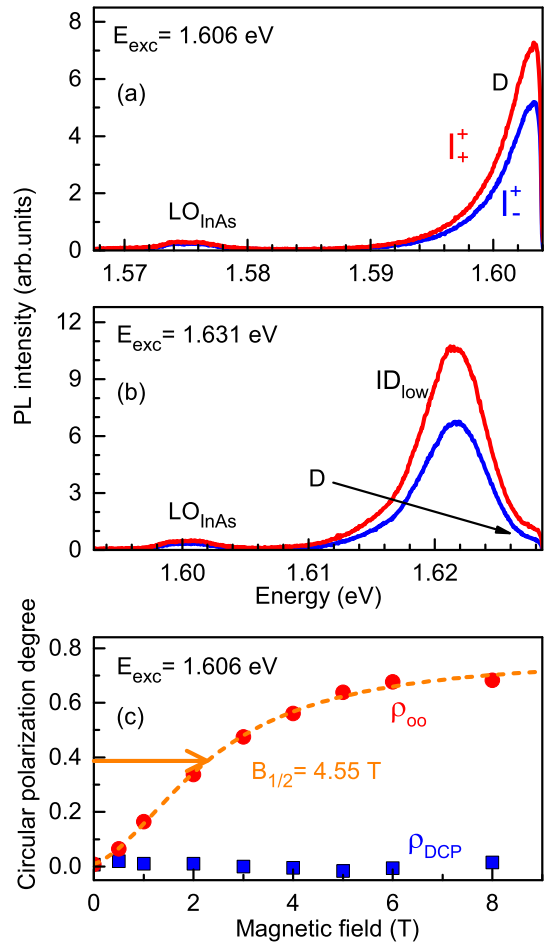

FIG. 4. Circular polarized PL intensities I_+^+ and I_-^+ for circular polarized excitation with (a) $E_{exc} < E_{\Gamma X}^{low}$ and (b) $E_{exc} > E_{\Gamma X}^{low}$. The longitudinal magnetic-field strength is $B = 1$ T (Faraday geometry). (c) Degree of circular polarization of the direct exciton emission (D line) for optical orientation (red dots) and DCP (blue squares) as a function of longitudinal magnetic field (Faraday geometry). The line shows the fit of experimental data with Eq. (5) using the fitting parameter $\delta_1 = (346 \pm 35)$ μeV. $T = 1.8$ K.

pure exciton spin states is lifted, and so the linear polarization decreases in favor of optical orientation [16]. In the general case, the circular polarization of the exciton emission in a longitudinal magnetic field for circularly polarized excitation is contributed by two components. The first one, ρ_{oo}, arises from the exciton spin polarization induced by optical orientation [17]. The second one, ρ_{DCP}, is induced by the thermal population of the exciton Zeeman levels with $|-1\rangle$ and $|+1\rangle$, provided by spin relaxation during the exciton lifetime [18–20].

The circular polarization degree of the D line can be calculated from the peak intensities of the PL spectra under circularly polarized excitation as shown in Fig. 4(a). The magnetic-field dependencies of ρ_{oo} and ρ_{DCP} measured at $E_{exc} = 1.606$ eV are presented in Fig. 4(c). One can see that the contribution by ρ_{DCP} is negligible due to the short exciton lifetime compared to its spin-relaxation time [5]. The circular polarization of the PL is determined by ρ_{oo} (red circles) and can be described by the following equation:

$$\rho_{oo}(B) = \rho_c^{max} \frac{(\mu_B g_{ex} B)^2}{\delta_1^2 + (\mu_B g_{ex} B)^2}, \quad (5)$$

with the maximal polarization ρ_c^{max} in strong fields, the Bohr magneton μ_B, and the longitudinal exciton g factor g_{ex}. The $\rho_{oo}(B)$ dependence is fitted well by a Lorentzian curve (dashed line) with FWHM $B_{1/2} = 4.55$ T. Taking into account the exciton g factor of $g_{ex} = 2.63$ [9,14], we can estimate the anisotropic exchange splitting from the following equation: $\delta_1 = \frac{1}{2} B_{1/2} \mu_B g_{ex}$ [9]. For an excitation energy of $E_{exc} = 1.606$ eV, we found $\delta_1 = (346 \pm 35)$ μeV.

In principle, it is possible to use the technique of restoring optical orientation to determine the anisotropic exchange splitting in any spectral range. However, in the spectral ranges where the intersection of the electronic Γ and X levels occur, the emission from direct and indirect band-gap QDs overlap strongly. This overlap hinders the determination of the circular

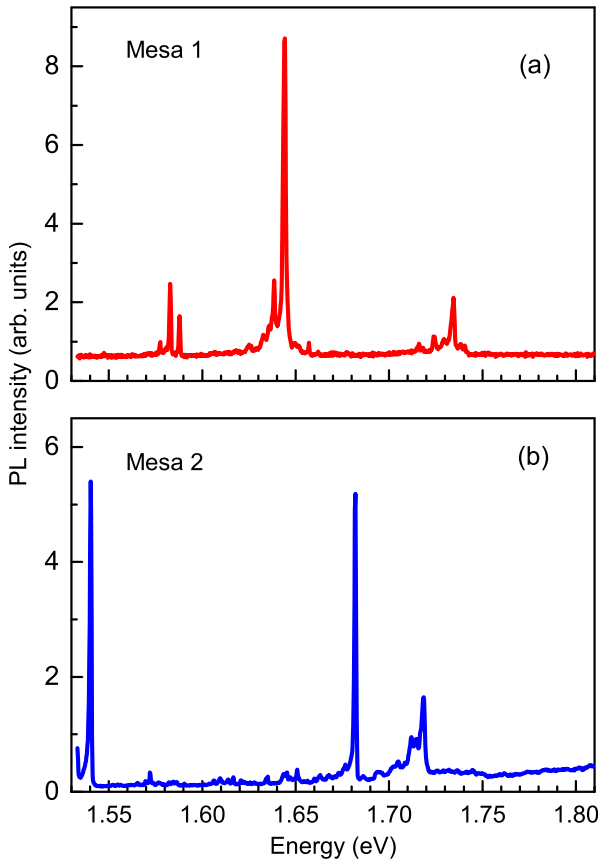

FIG. 5. Micro-PL spectra of (In,Al)As/AlAs QDs, measured on two different representative mesas. $T = 8$ K.

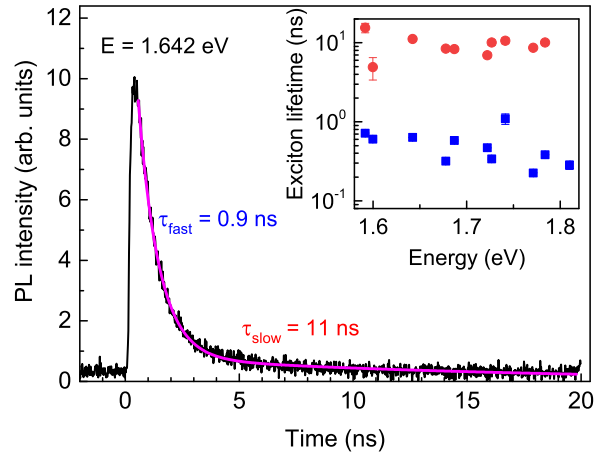

FIG. 6. Recombination dynamics of the PL line detected at 1.642 eV for $T = 8$ K. The biexponential fit is shown by the violet line. The inset shows the slow (red circles) and the fast (blue squares) time constants in dependence of detection energy.

polarization degree of the direct excitons. This is clearly seen for $E_{\text{exc}} > E_{\Gamma X}^{\text{low}}$ in Fig. 4(b) where the PL intensity of the direct transition is small compared to the indirect one.

B. Microphotoluminescence of single QDs

In order to determine the anisotropic exchange splitting also in QDs with mixed electronic levels Γ and X, we used the microphotoluminescence technique. Here, the sample with etched mesa structures was excited nonresonantly. Figure 5 shows the unpolarized PL spectra of two representative mesas. In contrast to the emission of the QD ensemble [Fig. 2(b)], the spectra from mesas show a number of narrow lines originating from individual QDs. It is known from Fig. 3(b) that the PL lines below 1.611 eV result from the recombination of direct QDs, whereas lines above this energy can be related to both direct or indirect QDs.

To reveal the origin of the narrow PL lines in the spectral region where the emission of the direct and indirect QDs coexists, we measured their recombination dynamics. The dynamics for a line detected at 1.642 eV is presented in Fig. 6. The decay curve reveals a two-component decay and is fitted by the sum of two exponential functions (red line) with lifetimes of $\tau_{\text{fast}} = 0.9$ and $\tau_{\text{slow}} = 11$ ns. These two time constants do not show any spectral variation as one can see in the inset of Fig. 6. Thus, even in the high-energy range, the recombination times are short compared to the lifetimes in the microsecond range, measured for indirect excitons. Therefore, we can conclude that the observed lines in the μPL spectra are associated with direct QDs and the recombination of electrons in the Γ valley of the conduction band with holes in the Γ valley of the valence band.

The radiative doublet of exciton states mixed by anisotropic exchange interaction $|X\rangle = \frac{1}{\sqrt{2}}(|+1\rangle + |-1\rangle)$ and $|Y\rangle = \frac{1}{i\sqrt{2}}(|+1\rangle - |-1\rangle)$ is dipole active along the two orthogonal principal axes of a QD [21]. Therefore, the exciton emission from a single QD is split into two cross-linearly polarized lines. Their energy splitting equals δ_1 [22], allowing direct measurement of the anisotropic exchange splitting.

Examples of single QD PL spectra with polarization axes perpendicular to each other (indicated by the blue and red colors) are shown in Figs. 7(a) and 7(b). In order to obtain the splitting value, we fit the data by Lorentz curves (not shown here). One can see that the energy shift between the PL maxima depends on the emission energy: For the emission at 1.5615 eV, the two lines are split by 602 μeV, whereas, at 1.6537 eV, the splitting is 53 μeV only. In order to assess the spectral dependence of δ_1, we measured the splitting for a set of single QDs emitting in the spectral range of 1.56–1.75 eV. The results are shown in Fig. 7(c) together with the δ_1 values obtained by the macro-PL technique (red triangles).

It turns out that the anisotropic exchange splitting has two minima at about 1.60 and 1.66 eV. At the first minimum δ_1 drops from 600 down to 80 μeV and then increases again up to 435 μeV. The absolute minimum of 53 μeV was measured close to 1.66 eV. For higher energies, the anisotropic exchange splitting increases again up to about 200 μeV.

C. Discussion

In direct band-gap QDs, the anisotropic exchange splitting of excitons depends strongly on geometrical factors and material properties. For the well-studied InAs/GaAs QDs, the δ_1 values vary typically in the range of 100–1000 μeV [23]. On the other hand, in indirect QDs, the exchange interaction is weak because the wave functions of the X electron and the Γ hole have very small overlap in momentum space [24,25].

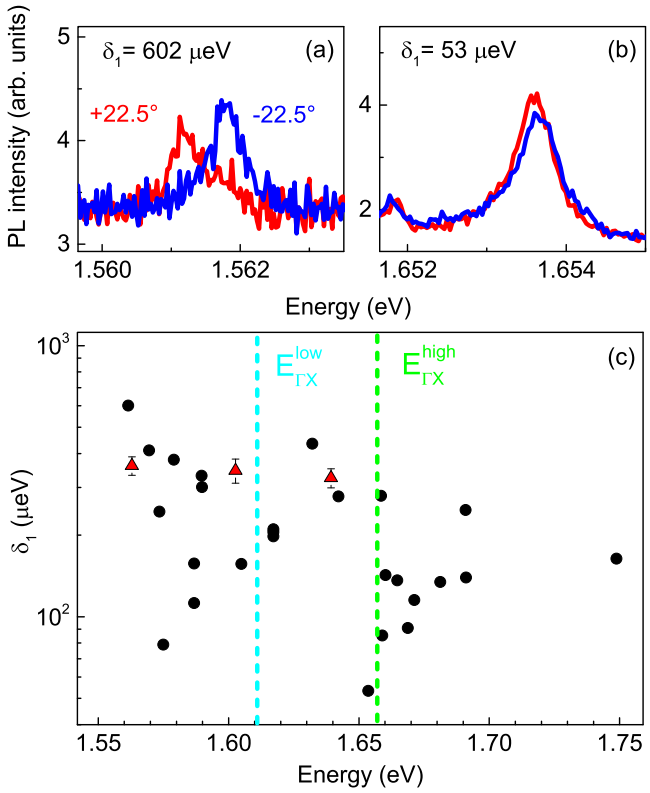

FIG. 7. (a) and (b) Linearly polarized PL spectra measured at two different energies under nonresonant excitation at $B = 0$ T. The angles $+22.5$ (red) and -22.5 (blue) of the $\lambda/2$ plate correspond to the x and y axes of the sample. (c) Spectral dependence of the anisotropic exchange splitting. The dashed lines show the positions of the ΓX-mixing energies. The results of the macroscopic measurement are indicated by red triangles. $T = 8$ K.

Since the energies of the δ_1 minima roughly correspond to the intersection energies of the Γ and X electron states [shown by the dashed lines in Fig. 7(c)], we can safely assume that the strong decrease in δ_1 can be explained by the ΓX mixing of the electron wave function.

In ideal bulk semiconductors, the electron states from the Γ and X valleys do not couple to each other, whereas ΓX mixing can take place in low-dimensional heterostructures (superlattices and QDs). It was shown that the intervalley electron transitions are provided by the uncertainty of the electron wave vector at the interfaces, which allows changes in the wave vector without interaction with phonons or defects [26,27].

We demonstrated recently that the violation of the translation symmetry in the xy plane of (In,Al)As/AlAs QDs results in ΓX mixing. The mixing is responsible for the strong variations of the exciton recombination rate by a thermal annealing treatment [11] and allows one to obtain resonant excitation of indirect electron states in the QDs [14]. Thus, an increase in the admixture of the X state to the electron wave function is expected to decrease the interaction of electron and hole states and, as a consequence, also the magnitude of the anisotropic exchange interaction.

IV. CONCLUSIONS

The anisotropic exchange splitting δ_1, caused by the interaction between Γ electrons and holes in (In,Al)As/AlAs QDs, was measured with a macroscopic and a microscopic technique. Both techniques deliver consistent results. However, only with the microscopic technique it is possible to measure δ_1 in the spectral range of the ΓX mixing. Here, the anisotropic exchange splitting decreases strongly due to the suppression of the electron-hole interaction.

ACKNOWLEDGMENTS

This work was supported by the Deutsche Forschungsgemeinschaft via Project No. 409810106 in the frame of the International Collaborative Research Center TRR 160 (Projects No. A1, No. B2 and No. C1) and by the Russian Foundation for Basic Research (Grants No. 19-52-12001 and No. 19-52-12057). A.A.T., M.V.R., and K.G.B. acknowledge support of the Russian Foundation for Basic Research (Grant No. 18-02-01212). T.S.S. acknowledges as well support of the Russian Foundation for Basic Research (Grant No. 19-02-00098) as well as the Government of the Russian Federation via Act 211 (Contract No. 02.A03.21.0006) and Grant No. AAAA-A17-117042110141-5.

[1] *Optics of Semiconductors and Their Nanostructures*, edited by H. Kalt and M. Hetterich (Springer-Verlag, Berlin, 2004).

[2] C. F. Klingshirn, *Semiconductor Optics* (Springer-Verlag, Heidelberg, 2012).

[3] M. Bayer, G. Ortner, O. Stern, A. Kuther, A. A. Gorbunov, A. Forchel, P. Hawrylak, S. Fafard, K. Hinzer, T. L. Reinecke, S. N. Walck, J. P. Reithmaier, F. Klopf, and F. Schäfer, Fine structure of neutral and charged excitons in self-assembled In(Ga)As/(Al)GaAs quantum dots, Phys. Rev. B **65**, 195315 (2002).

[4] E. L. Ivchenko and G. E. Pikus, *Superlattices and other Heterostructures*, Springer Series in Solid-State Sciences Vol. 110 (Springer-Verlag, Berlin, 1997).

[5] M. Paillard, X. Marie, P. Renucci, T. Amand, A. Jbeli, and J. M. Gérard, Spin Relaxation Quenching in Semiconductor Quantum Dots, Phys. Rev. Lett. **86**, 1634 (2001).

[6] L. Besombes, K. Kheng, and D. Martrou, Exciton and Biexciton Fine Structure in Single Elongated Islands Grown on a Vicinal Surface, Phys. Rev. Lett. **85**, 425 (2000).

[7] T. S. Shamirzaev, A. V. Nenashev, and K. S. Zhuravlev, Coexistence of direct and indirect band structures in arrays of InAs/AlAs quantum dots, Appl. Phys. Lett. **92**, 213101 (2008).

[8] T. S. Shamirzaev, A. V. Nenashev, A. K. Gutakovskii, A. K. Kalagin, and K. S. Zhuravlev, Atomic and energy structure of InAs/AlAs quantum dots, Phys. Rev. B **78**, 085323 (2008).

[9] J. Rautert, T. S. Shamirzaev, S. V. Nekrasov, D. R. Yakovlev, P. Klenovský, Y. G. Kusrayev, and M. Bayer, Optical orientation

and alignment of excitons in direct and indirect band gap (In,Al)As/AlAs quantum dots with type-I alignment, Phys. Rev. B **99**, 195411 (2019).

[10] M. Bayer, A. Kuther, A. Forchel, A. Gorbunov, V. B. Timofeev, F. Schäfer, J. P. Reithmaier, T. L. Reinecke, and S. N. Walck, Electron and Hole g Factors and Exchange Interaction from Studies of the Exciton Fine Structure in $In_{0.60}Ga_{0.40}As$ Quantum Dots, Phys. Rev. Lett. **82**, 1748 (1999).

[11] T. S. Shamirzaev, J. Debus, D. S. Abramkin, D. Dunker, D. R. Yakovlev, D. V. Dmitriev, A. K. Gutakovskii, L. S. Braginsky, K. S. Zhuravlev, and M. Bayer, Exciton recombination dynamics in an ensemble of (In,Al)As/AlAs quantum dots with indirect band-gap and type-I band alignment, Phys. Rev. B **84**, 155318 (2011).

[12] V. Y. Ivanov, T. S. Shamirzaev, D. R. Yakovlev, A. K. Gutakovskii, Ł. Owczarczyk, and M. Bayer, Optically detected magnetic resonance of photoexcited electrons in (In,Al)As/AlAs quantum dots with indirect band gap and type-I band alignment, Phys. Rev. B **97**, 245306 (2018).

[13] T. S. Shamirzaev, D. S. Abramkin, A. V. Nenashev, K. S. Zhuravlev, F. Trojanek, B. Dzurnak, and P. Maly, Carrier dynamics in InAs/AlAs quantum dots: Lack in carrier transfer from wetting layer to quantum dots, Nanotechnology **21**, 155703 (2010).

[14] J. Debus, T. S. Shamirzaev, D. Dunker, V. F. Sapega, E. L. Ivchenko, D. R. Yakovlev, A. I. Toropov, and M. Bayer, Spin-flip Raman scattering of the Γ-X mixed exciton in indirect band gap (In,Al)As/AlAs quantum dots, Phys. Rev. B **90**, 125431 (2014).

[15] *Physics of Group IV Elements and III-V Compounds*, edited by O. Madelung, M. Schulz, and H. Weiss, Landolt-Börnstein Numerical Data and Relationships, New Series, Group III Vol. 17, Pt. a (Springer, Berlin, 1982).

[16] R. I. Dzhioev, H. M. Gibbs, E. L. Ivchenko, G. Khitrova, V. L. Korenev, M. N. Tkachuk, and B. P. Zakharchenya, Determination of interface preference by observation of linear-to-circular polarization conversion under optical orientation of excitons in type-II GaAs/AlAs superlattices, Phys. Rev. B **56**, 13405 (1997).

[17] *Optical Orientation*, edited by F. Meier and B. P. Zakharchenja (North-Holland, Amsterdam, 1984).

[18] T. S. Shamirzaev, Exciton recombination and spin dynamics in indirect-gap quantum wells and quantum dots, Phys. Solid State **60**, 1554 (2018).

[19] T. S. Shamirzaev, J. Rautert, D. R. Yakovlev, J. Debus, A. Y. Gornov, M. M. Glazov, E. L. Ivchenko, and M. Bayer, Spin dynamics and magnetic field induced polarization of excitons in ultrathin GaAs/AlAs quantum wells with indirect band gap and type-II band alignment, Phys. Rev. B **96**, 035302 (2017).

[20] T. S. Shamirzaev, J. Debus, D. R. Yakovlev, M. M. Glazov, E. L. Ivchenko, and M. Bayer, Dynamics of exciton recombination in strong magnetic fields in ultrathin GaAs/AlAs quantum wells with indirect band gap and type-II band alignment, Phys. Rev. B **94**, 045411 (2016).

[21] D. Gammon, E. S. Snow, B. V. Shanabrook, D. S. Katzer, and D. Park, Fine Structure Splitting in the Optical Spectra of Single GaAs Quantum Dots, Phys. Rev. Lett. **76**, 3005 (1996).

[22] E. L. Ivchenko, Fine structure of excitonic levels in semiconductor nanostructures, Phys. Stat. Solidi A **164**, 487 (1997).

[23] R. Seguin, A. Schliwa, S. Rodt, K. Pötschke, U. W. Pohl, and D. Bimberg, Size-Dependent Fine-Structure Splitting in Self-Organized InAs/GaAs Quantum Dots, Phys. Rev. Lett. **95**, 257402 (2005).

[24] G. E. Pikus and G. L. Bir, Exchange interaction in excitons in semiconductors, Zh. Eksp. Teor. Fiz. **60**, 195 (1971) [Sov. Phys. JETP **33**, 108 (1971)].

[25] G. L. Bir and G. E. Pikus, *Symmetry and Strain-Induced Effects in Semiconductors* (Wiley, New York, 1974).

[26] R. J. Teissier, J. J. Finley, M. S. Skolnick, J. W. Cockburn, J.-L. Pelouard, R. Grey, G. Hill, M. A. Pate, and R. Planel, Experimental determination of Γ-X intervalley transfer mechanisms in GaAs/AlAs heterostructures, Phys. Rev. B **54**, R8329(R) (1996).

[27] Y. Fu, M. Willander, E. L. Ivchenko, and A. A. Kiselev, Valley mixing in GaAs/AlAs multilayer structures in the effective-mass method, Phys. Rev. B **47**, 13498 (1993).